NANO LETTERS

2007
Vol. 7, No. 11
3462−3468

Supported Lipid Bilayer Formation and Lipid-Membrane-Mediated Biorecognition Reactions Studied with a New Nanoplasmonic Sensor Template

Magnus P. Jonsson, Peter Jönsson, Andreas B. Dahlin, and Fredrik Höök*

Division of Solid State Physics, Lund University, SE-22100 Lund, Sweden

Received August 11, 2007; Revised Manuscript Received September 13, 2007

ABSTRACT

This paper presents the use of the localized surface plasmon resonance (LSPR) sensor concept to probe the formation of macroscopic and laterally mobile supported lipid bilayers (SLBs) on SiO_x-encapsulated nanohole-containing Au and Ag films. A comparison between Au- and Ag-based sensor templates demonstrates a higher sensitivity for Au-based templates with respect to both bulk and interfacial refractive index (RI) changes in aqueous solution. The lateral mobility of SLBs formed on the SiO_x-encapsulated nanohole templates was analyzed using fluorescence recovery after photobleaching (FRAP), demonstrating essentially complete (>96%) recovery, but a reduction in diffusivity of about 35% compared with SLBs formed on flat SiO_x substrates. Furthermore, upon SLB formation, the temporal variation in extinction peak position of the LSPR active templates display a characteristic shape, illustrating what, to the best of our knowledge, is the first example where the nanoplasmonic concept is shown capable of probing biomacromolecular structural changes without the introduction of labels. With a signal-to-noise ratio better than 5×10^2 upon protein binding to the cell-membrane mimics, the sensor concept is also proven competitive with state-of-the-art label-free sensors.

Around one-third of the human proteins are associated with cell membranes. There they orchestrate key functions in living cells, and it is therefore not surprising that more than half of the existing drugs are directed toward membrane-residing proteins. A key component of the natural cell membrane is their inherent lateral mobility, which allows for lipids, proteins, and other membrane components to colocalize in order to regulate, for example, membrane protein-mediated transport across the cell membrane or to ensure the formation of essential protein complexes. Connected with the lateral mobility of cell membranes is also the formation of lipid domains, which are believed to play an essential role in, for example, membrane fusion events as well as in the pathogenesis of several diseases.[1−5] Fluidity in the cell membrane is also widely utilized in nature to increase binding affinities through multivalent interactions.[6]

One type of artificial mimic of the natural cell membrane that has attracted significant attention recently is so-called supported lipid bilayers (SLBs).[7−9] This is in part due to their compatibility with protein incorporation[7,10,11] but also the fact that they, under the right conditions, possess sustained lateral mobility.[7,12,13] SLBs can be formed from a wide range of lipid compositions and can be supported on several different materials, including unmodified or chemically modified metals[14,15] and metal oxides.[16] However, silica-based materials are, together with mica, by far the most commonly used substrates. Besides providing SLBs with a lateral mobility that resembles that of the natural cell membrane,[7] the popularity of these supports is due to their compatibility with simple preparation procedures of SLBs. In fact, without any surface modification, apart from sufficient cleaning, macroscopic SLBs can be spontaneously formed from the adsorption, and subsequent rupture, of suspended small unilamellar phospholipid vesicles (SUVs).[7,9,11,17,18] To mention a few examples, it has been shown that SLBs provide suitable templates for studies of membrane proteins,[11] crystallization of water soluble proteins,[19−23] and multivalent binding reactions.[24,25]

Spontaneous formation of SLBs from adsorption of suspended SUVs has been under extensive investigation during the past decades. In these studies, various fluorescence microscopy techniques have been widely utilized.[7,18,26−28] Examples of other methods, which do not require labeling of lipids, are scanning probe microscopy (SPM),[29,30] surface plasmon resonance (SPR),[31,32] and ellipsometry.[33] The quartz crystal microbalance with dissipation (QCM-D) monitoring technique is another label-free technique that has been extensively used due to the unique signature it provides to verify successful SLB formation.[17,31] In addition, the lateral mobility of SLBs is often analyzed using fluorescence

* Corresponding author. E-mail: fredrik.hook@ftf.lth.se. Telephone: +46-46-2221494. Fax: +46-46-2223637.

10.1021/nl072006t CCC: $37.00
Published on Web 09/29/2007

recovery after photobleaching (FRAP)[7,34,35] or fluorescence correlation spectroscopy (FCS),[12,36] which both provide sufficient information to determine a diffusion coefficient characterizing the mobility of the labeled lipids in the SLB.

The label-free techniques mentioned above are also extremely attractive when SLBs are used as sensor platforms to probe membrane-mediated biorecognition reactions. Because of the high relevance of cell-membrane mimics in diagnostics and drug screening, there is currently an eager search for new sensor concepts compatible with studies of SLBs.[37] One of the most exciting label-free sensing concepts is the so-called localized surface plasmon resonance (LSPR), which lately has been utilized in a number of different sensor applications.[38−48] In brief, LSPR is a phenomenon that arises when the conduction electrons in a metal nanostructure couples with the field oscillations of electromagnetic waves. This coupling gives rise to a characteristic optical extinction spectrum,[49] which is strongly dependent on the choice of metal, the geometry of the nanostructures, and the substrate material.[50−53] In addition, the position and the magnitude of the extinction peak are highly dependent on the refractive index of the vicinity of the metal nanostructures.[50−54] This can, in turn, be used to probe changes of the refractive index in close proximity to the nanostructures, which forms the basis for the use of the LSPR phenomenon for label-free affinity-based sensing applications.

Since Englebienne et al. in 1998 demonstrated end-point sensing of biorecognition reactions using LSPR,[47] the concept has been extended to, for example, real-time studies of specific binding of proteins and antibodies,[48] detection of DNA hybridization,[55] sensing of biomarkers for Alzheimer's disease,[39] imaging as well as treatment of cancer cells,[56−59] and analysis of recombinant protein expression.[60] Furthermore, the sensor concept has been proven compatible with analysis of down to single nanostructures.[61−63] This, together with the fact that the LSPR field is extremely confined around the nanostructures,[62,64] points toward the exiting opportunity of high-density array-based sensing, with several applications within high-throughput diagnostics and drug screening.

On the basis of selective surface modification of Au and SiO_2, our group recently extended the LSPR sensing concept to monitor lipid-membrane-mediated biorecognition reactions using either SLB patches[38] or DNA-tethered SUVs[65] confined in nanometric plasmon active apertures in thin (15−55 nm) Au films on transparent SiO_2 substrates. In the study presented in this paper, the aim was to extend these efforts toward a nanoplasmonic sensor compatible with studies of macroscopic SLBs with preserved long-range lateral mobility. This challenge was addressed by preparing LSPR active nanoholes in either thin Au and Ag films, which were subsequently encapsulated in thin silicon oxide (SiO_x) films, as schematically illustrated in Figure 1. Besides providing a protective layer for the easily oxidized Ag film, thus enabling a fair comparison between the Au and Ag materials in terms of sensing capability, the SiO_x coating was chosen to promote spontaneous SLB formation upon adsorption of SUVs. In addition, the extended SiO_x coating eliminates the need for

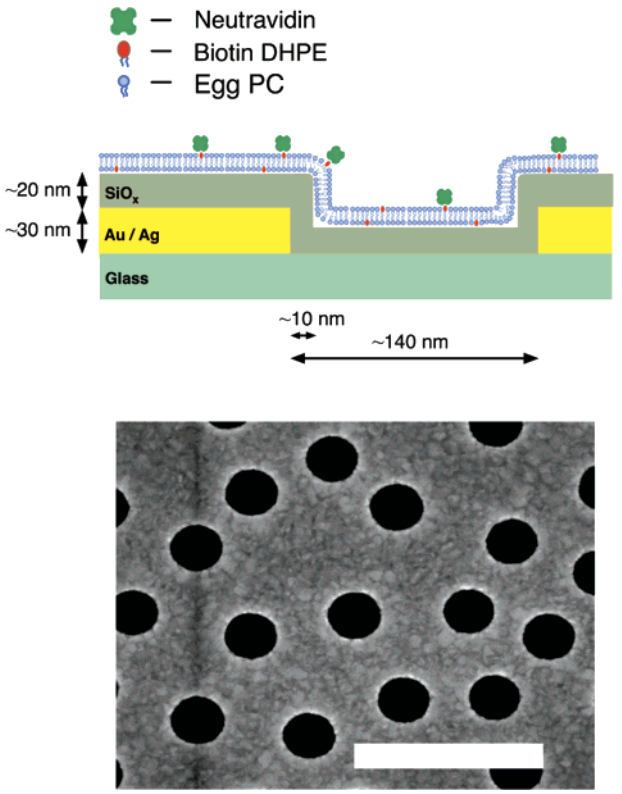

Figure 1. Schematic illustration of the LSPR nanosensor (top). Also shown is a scanning electron micrograph of a typical Au sample after lift off (bottom). The scale bar is 500 nm.

selective surface modifications of the metal and the substrate. Finally, it prevents signals generated from nonspecific binding to adhesion layers (e.g., Cr or Ti) between the metal and the substrate, which have been reported as a possible limitation of LSPR nanosensors.[39,66]

Samples with SiO_x-encapsulated Au or Ag nanoholes were fabricated using a modified version of colloidal lithography[67] and characterized as described in the Supporting Information. Optical extinction spectra acquired in air before and after sputtering of roughly 20 nm SiO_x demonstrate significant red-shifts of the peak positions, λ_{peak}, both for Ag and Au samples (Figure 2A). Together with scanning electron microscopy (SEM) inspections of the nanoholes (see Supporting Information), the observed red-shifts, which are similar to those previously reported for encapsulated Ag nanoparticles,[49] confirm efficient coating with SiO_x. The variation in peak position ($\Delta\lambda_{peak}$) as a function of refractive index (RI) of the surrounding medium was determined by acquiring extinction spectra in air, water, and different concentrations of glycerol dissolved in water (0−35 wt % in steps of 5%). In agreement with previously reported results for Ag nanostructures,[44,68] repeated measurements on Ag samples showed a linear relation between $\Delta\lambda_{peak}$ and ΔRI in the RI interval from 1 to 1.37, both without (blue in Figure 2C) and with (blue in Figure 2D) SiO_x. In contrast, data obtained for Au samples showed nonlinear behaviors in the same RI interval both without (red in Figure 2C) and with (red in Figure 2D) SiO_x coating. For SiO_x-encapsulated holes in Au, the nonlinear relation was confirmed using *p*-xylene with a RI of approximately 1.50 (not shown).

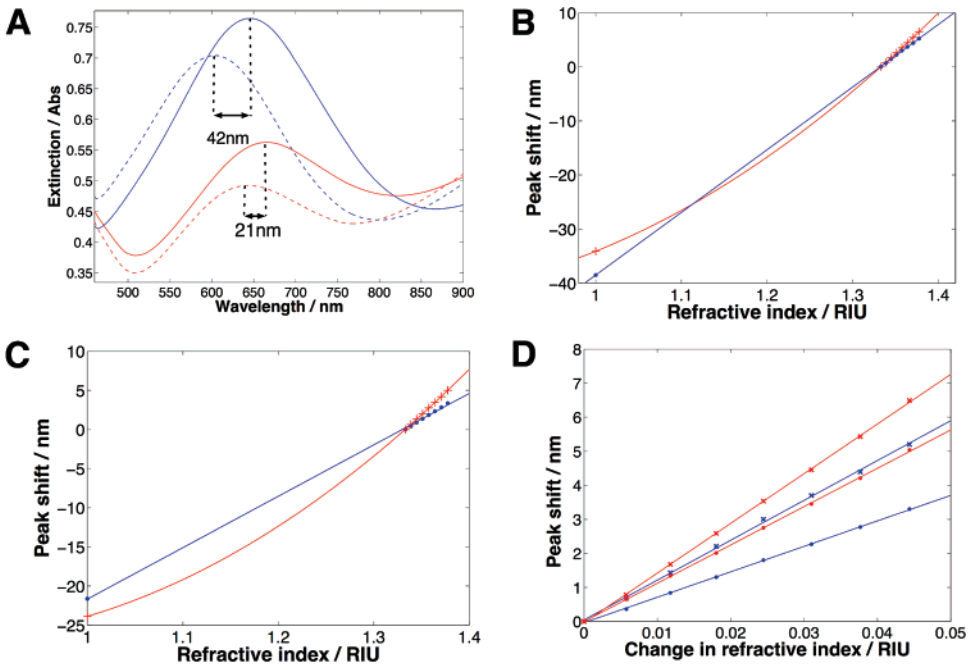

Figure 2. (A) Extinction spectra obtained in air of nanohole-modified (diameter 140 nm, depth 30 nm) Au (red) and Ag (blue) samples without (dashed lines) and with (solid lines) ~20 nm sputtered SiO_x. (B) Variation in peak position vs refractive index for Au (red) and Ag (blue) samples without SiO_x measured in air, water, and different concentrations of glycerol in water (0−35 wt %). Crosses and dots represent experimental data, and the solid lines are polynomial fits made to help the eye. The peak shifts are chosen to be zero in pure water. (C) Same as in (B) but for holes encapsulated in SiO_x. (D) Enlarged curves from (B) and (C) illustrating the sensitivities around a refractive index of 1.333. The sensitivities are defined as the slopes from linear fits to peak shifts vs changes in refractive index of the surrounding medium (solid lines).

Because the slope of the $\Delta\lambda_{peak}$ versus ΔRI curve defines the bulk sensitivity of the sensor, these results imply that Ag samples have approximately constant sensitivity over the investigated RI interval, while the sensitivity of the Au samples increases with RI. In fact, the red-shift (obtained in air) induced upon SiO_x deposition is approximately a factor of 2 larger for the Ag sample (42 nm) than the red-shift for the Au sample (21 nm) (Figure 2A). This, together with the fitted curves in Figure 2B,C, implies that in air, the Au sample is significantly less sensitive than the Ag sample, while in contrast, the sensitivities measured around an RI of 1.333 (Figure 2D) are higher for Au samples than for Ag samples, both without (146 nm/RIU compared with 117 nm/RIU) and with (113 nm/RIU compared with 75 nm/RIU) the SiO_x coating. In fact, the SiO_x-encapsulated Au sample has approximately 50% higher sensitivity than the identically encapsulated Ag sample when measured around the refractive index of water.

The observed differences between the Au and the Ag samples can in part be understood from differences between the optical dielectric functions of the materials. For discontinuous metal nanostructures such as nanospheres and nanodisks, the resonance condition can be described by:[54,69]

$$\mathrm{Re}(\epsilon(\lambda_{peak})) = -\gamma n^2 \qquad (1)$$

where $\epsilon(\lambda_{peak})$ is the dielectric function of the metal at the wavelength of maximum extinction, λ_{peak}. γ is a shape factor that depends on the geometry, and n is the refractive index of the surrounding medium. Kall et al. showed in a recent paper[69] that eq 1 qualitatively describes the optical resonance phenomenon also for nanometric holes. Following this argumentation, tabulated dielectric data from Johnson and Christy[70] suggest that, for Ag, there is a roughly linear increase in peak position with respect to refractive index (Figure S2 in Supporting Information), whereas for Au, there is an approximately quadratic dependence (Figure S2 in Supporting Information). Qualitatively, this confirms the experimental observations for both uncoated and SiO_x-coated nanoholes (Figure 2C,D). However, a full quantitative explanation of the LSPR phenomena associated with the nanostructures presented in this paper requires a complete theoretical description of the randomized hole structure, presumably taking into account also differences in grain size of the evaporated Au and Ag, the actual peak positions,[54] variation in hole shape induced by cleaning methods, weak oxidation of Ag, etc. (see Supporting Information). Nevertheless, it can be concluded that, under our experimental conditions, the Au sample is the most sensitive one at a refractive index close to or above that of water. This, in turn, points toward Au as the preferable choice for studies of biorecognition reactions under physiological conditions, although, in terms of measuring variation in peak position with high accuracy and high temporal resolution, the actual peak shape also plays an important role (see further below).

To extend the comparison of the SiO_x-encapsulated Au and Ag samples, the sensitivity was evaluated with respect to SLB formation under conditions at which this is a spontaneous process on homogeneous silica. To analyze SLB

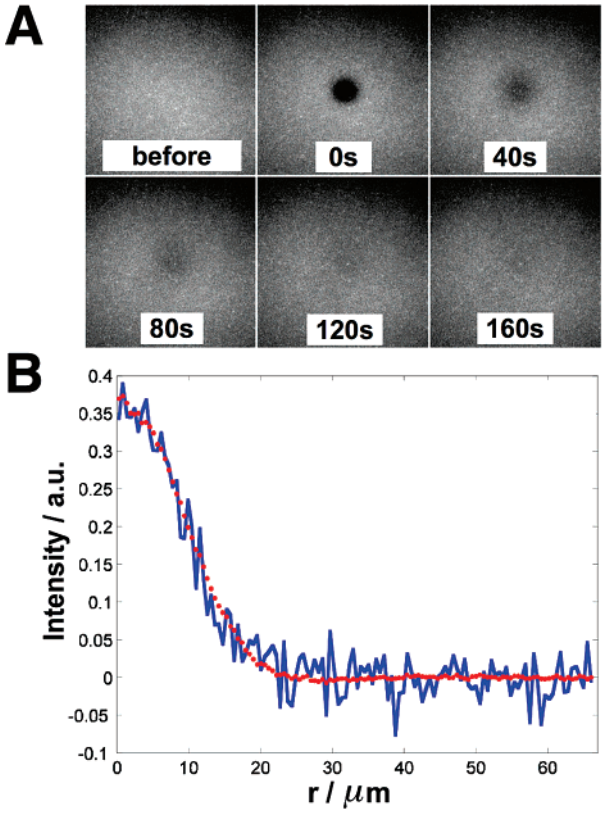

Figure 3. (A) Fluorescence micrographs from a typical FRAP experiment showing fluorescence recovery for a SLB on SiO_x-encapsulated Au holes. Images for the montage are picked from the acquired FRAP sequence and chosen before, directly after, 40 s after, 80 s after, 120 s after, and 160 s after bleaching (B) Typical bleaching profiles before (blue) and after averaging (red) of the fluorescence intensities at constant radial values. The intensity used in the figure is the difference between a prebleach image and the bleached images, i.e., bleached regions have higher values than nonbleached regions.

formation on samples with SiO_x-encapsulated nanoholes, suspended SUVs with a small fraction (1%) of fluorescently labeled lipids (rhodamine-DHPE) were added to the sensor template. After rinsing with buffer, SLB formation was examined with FRAP. Figure 3A shows typical fluorescence images of a SLB formed on SiO_x-encapsulated Au holes (similar results were obtained for SiO_x-encapsulated Ag holes). On both substrates, the fraction of nonmobile fluorophores was less than 0.04 (with 95% upper confidence bound), which is small even compared with SLBs formed on atomically flat mica. This means that an insignificant amount of rhodamine-DHPE molecules were spatially restricted to micro- or nanoscopic regions of the sample. If the SLB formation would have been significantly disrupted by the presence of nanoholes, which constitute about 15% of the projected surface area, the fraction of nonmobile lipids would have been significantly larger due to immobile lipids associated with the holes. Therefore, these results strongly support formation of a continuous SLB across the holes. In addition, comparing the total intensity of the prebleached images from surfaces with holes and reference regions with flat sputtered SiO_x without holes yields a 20% higher total fluorescence intensity for the regions with holes (data not shown). This is interpreted as originating from lipid bilayer formation also on the sidewalls of the holes.

The diffusion coefficient (D) of rhodamine-DHPE lipids in SLBs were determined by FRAP. The analysis method, briefly described in the Supporting Information, takes advantage of the approximately circular symmetry of the bleaching spot by averaging the image for constant radial values for each frame in the image sequence. This yields a significant decrease in the noise level for the radial intensity, as illustrated in Figure 3B, and improves a comparison of different regions on the same sample. The diffusion coefficient for SiO_x-encapsulated Au holes (the image sequence in Figure 3A) was determined to $0.99 \pm 0.03\ \mu m^2/s$, where the standard deviation is estimated from determining D on different regions on the sample. Despite essentially full recovery on regions both with and without holes (see above), this value is about 65% of the value obtained on flat regions with sputtered SiO_x on the same sample ($D = 1.52 \pm 0.04\ \mu m^2/s$). While the latter value is comparable to previously published values of the diffusion coefficient of fluorescent lipids in SLBs on glass,[35] the former value signals, in agreement with previous reports for structured supports,[71] a reduction in diffusivity within the SLB on the hole region. A decrease in the diffusion coefficient is in the present case expected if fluorophores, besides diffusing between holes, also can diffuse into the holes. The additional area produced by the sidewalls of the holes yields a larger effective area and therefore a proportional reduction in diffusivity. Note, however, that the effective area for the regions with nanoholes is only 15% larger than that of a flat surface, which means that the larger area cannot fully account for the reduced diffusivity. Therefore, also, other plausible effects, such as reduced lateral mobility due to the high curvature of the SLB near the edges of the holes, may contribute to the observed reduction in diffusivity.

The results from the fluorescence experiments confirm formation of a mobile SLB across the nanoholes. In addition, the results show that the effective surface area of the SLB is larger than that of a SLB formed on a flat surface, consistent with a SLB that firmly follows the nanostructure. The detailed structure of the lipid bilayer inside the nanoholes will, to a first approximation, be determined by a balance between the gain in energy due to adhesion, $E_{adhesion}$, and the energy cost associated with bending of the bilayer, E_{bend}. The adhesion energy is described by:[72]

$$E_{adhesion} = -W \cdot A_{adhesion} \tag{2}$$

where W is the adhesion potential and $A_{adhesion}$ is the area in contact with the substrate. The counteracting bending energy for a lipid bilayer can be approximated by:[72]

$$E_{bend} \approx \frac{1}{2}\kappa_{bend}\left(\frac{1}{r_1} + \frac{1}{r_2}\right)^2 A_{bend} \tag{3}$$

where r_1 and r_2 are the radii of the curvature, κ_{bend} is the bending modulus for the lipid bilayer, which is approximately 5×10^{-20} J,[72] and A_{bend} is the area of the curved region.

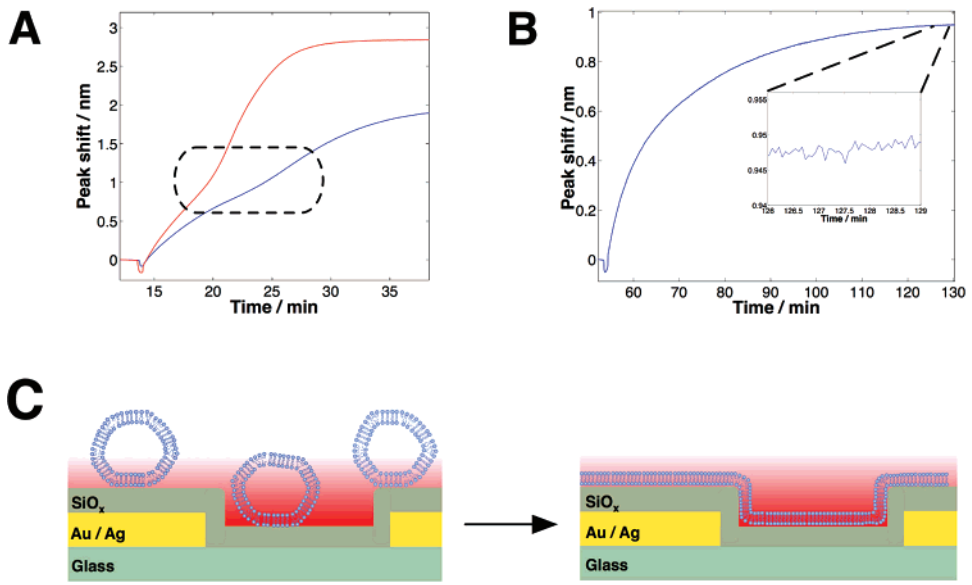

Figure 4. (A) Changes in peak position vs time upon addition of suspended SUVs ($t \sim 13$ min) to SiO_x-encapsulated Au (red) and Ag (blue) nanohole samples. The black dashed line marks the signature for SLB formation (see main text). (B) The same type of data as in (A) upon addition of Neutravidin (10 μg/mL) to a SLB functionalized with 1% biotinylated lipids. The inset illustrates the noise level (better than 0.002 nm). (C) Schematic illustration of the movement of lipids upon rupture of adsorbed SUVs (left) into an extended SLB (right). The fading red region illustrates the rapidly decaying LSPR field. Not drawn to scale.

There are reported values for the adhesion potential ranging from 0.15 to 3.5 mJ/m^2.[30,72] By setting $E_{adhesion} = E_{bend}$ and assuming that $A_{adhesion}$ equals A_{bend}, these reported values correspond to radii ($r_1 = r_2$) in a range between 5 and 26 nm, which is considerably smaller than the dimensions of the holes. This, together with the results from the fluorescence experiments, including the reduced diffusivity, strongly suggests that the bilayer roughly follows the structure of the holes as depicted schematically in Figure 1.

To analyze the optical response of the LSPR active samples under conditions where SLB formation was proven successful, the temporal variation of λ_{peak} upon addition of SUVs to SiO_x-encapsulated Au and Ag samples was measured by acquiring LSPR spectra continuously as described previously.[38] Figure 4A shows $\Delta\lambda_{peak}$ versus time upon SLB formation on SiO_x-encapsulated Au (red) and Ag (blue) samples. After addition of suspended SUVs ($t \sim 13$ min), there is an instantaneous decrease in λ_{peak}. This is attributed to a weak wavelength dependence of the scattering properties of suspended SUVs in solution, as confirmed by an equal increase in peak position upon rinsing with buffer (not shown). The instantaneous decrease is followed by a monotonic increase in $\Delta\lambda_{peak}$, attributed to adsorption of SUVs. At around 7 min (red) and 10 min (blue), after addition of SUVs, the responses display slow but significant accelerations resulting in kink-shaped curves. Finally, the peak shifts saturate at around 3 and 2 nm for the SiO_x-encapsulated Au and Ag samples, respectively. In agreement with the evaluation of the sensitivity to changes in bulk RI, these results show that the Au sample possesses a higher sensitivity (roughly 50%) compared to the Ag sample also upon changes in interfacial RI induced by biomolecular binding in aqueous solutions. However, because of a better-defined peak for the Ag samples compared with the Au samples (Figure 2A), the advantage in terms of signal-to-noise ratio of the Au sample over the Ag sample is less significant. Despite the fact that the sensitivity was reduced by the SiO_x coating, the saturated peak position shift upon lipid bilayer formation was higher for SiO_x-coated holes than for noncoated holes (Au) with similar geometry but where the gold was made inert using thiol chemistry (unpublished data). This is attributed to the larger sensing volume occupied by lipids upon bilayer formation also on the sides of the SiO_x-coated holes. The observation is in agreement with the results from the fluorescence experiments.

Interestingly, repeated combined LSPR and FRAP measurements on SiO_x-encapsulated Au and Ag samples confirmed a good correlation between the characteristic shape of the LSPR curve and successful formation of SLBs with high lateral mobility. On those occasions when, due to insufficient cleaning, no or weak recovery was observed, the temporal variation in $\Delta\lambda_{peak}$ was essentially monotonic toward saturated binding (not shown). Together, these two observations confirm that the characteristic shape of the response is attributed to successful SLB formation.

To explain this peculiar observation, one must recall that the intensity of the evanescent field is highest at, and decays rapidly away from, the sensor surface.[62,64] Furthermore, spontaneous SLB formation from adsorption of SUVs on silica proceeds via an initial adsorption of unruptured SUVs, which at a critical coverage of about 30% start to rupture into an extended SLB.[73,74] During the vesicle-rupture process, lipids associated with adsorbed SUVs move closer to the surface and thereby into a region where the LSPR field strength is higher (see schematic illustration in Figure 4C). As a consequence, the magnitude of $\Delta\lambda_{peak}$ at a given time interval is expected to have a positive contribution from not only adsorption of SUVs but also vesicle rupture. Hence, the observed acceleration in the LSPR response is attributed not to an increase in the actual mass deposition but to a

structural change of the already adsorbed SUVs. A similar observation was previously made upon SLB formation measured using conventional SPR,[74] although the considerably longer decay length of the evanescent fields associated with SPR compared with LSPR[41,75] made the signature significantly weaker in that case. The plasmonic coupling between gold colloids that are mobile with respect to each other have been used previously to probe biomacromolecular structural changes,[76] as has changes in fluorescence quenching of fluorophores coupled to biomolecules immobilized on SPR active templates.[27] However, to the best of our knowledge, this is the first example illustrating the use of the shallow evanescent field of LSPR active templates to probe biomacromolecular structural changes without the introduction of external labels.

Finally, the capacity of the sensor platform for studies of biorecognition reactions was evaluated by functionalizing the SLB with a small fraction (1%) of biotinylated lipids. This allows for subsequent capturing of avidin or its analogues streptavidin and Neutravidin, as schematically illustrated in Figure 1. The introduction of biotinylated lipids did not influence the signature for bilayer formation, and upon subsequent addition of Neutravidin (10 μg/mL), a monotonic binding curve that saturates at a peak position shift of $\sim$1 nm (Au sample) was observed (Figure 4B). Compared with the sample without the SiO_x coating, the (bulk) sensitivity was reduced by a factor of $\sim$1.3 by the SiO_x coating (Figure 2D) and most likely somewhat further by the presence of the SLB. Still, the response obtained upon Neutravidin binding demonstrates that the sensor platform is capable of probing protein binding in real time (repetition rate better than 2 s) with a high signal-to-noise ratio. In fact, with a noise of $\sim 2 \times 10^{-3}$ nm (inset in Figure 4B), the signal-to-noise ratio is approximately 5×10^2, which is high also compared with state-of-the-art label-free sensor platforms.

In conclusion, the already-proven compatibility of the nanoplasmonic concept with extreme miniaturization, proven efficient all the way down to the level of single particles and holes,[61−63] makes the extension of the LSPR sensing concept to laterally mobile SLBs highly interesting with respect to analysis of single membrane-mediated biorecognition events without the introduction of external labels. For multiplexity, SLBs on array-based format could be realized following the brute force approach suggested by Lahiri and co-workers,[14] who have demonstrated successful SLB formation in an array format using conventional ink-jet dispensing. Another promising alternative is the integration with microfluidics for selective functionalization of closely situated membrane compartments.[77] SLBs in one-dimensional arrays could be simultaneously probed in real time by acquiring spectral information on one axis and spatial information on the other,[45] while two-dimensional arrays could be investigated by microspectrometry in scanning mode or in a simultaneous fashion at one or a few given wavelengths using a CCD and a motorized filter wheel. This makes us confident in the belief that the sensor concept presented in this paper can be successfully extended to multiplexed sensing and even array-based high-throughput drug screening. From a pure fundamental perspective, we also emphasize the relevance of the characteristic shape of the LSPR response obtained upon SLB formation. In combination with complementary techniques, such as AFM, QCM-D, surface plasmon resonance-enhanced fluorescence, impedance spectroscopy, etc., we foresee a new means to characterize both surface-induced and biorecognition-induced structural changes of biomacromolecules.

Acknowledgment. We gratefully thank Dr. Jonas Tegenfeldt for experimental support. The work was financially supported by the Swedish Research Council for Engineering Sciences, contract number 2005-3140, and the Ingvar grant from the Strategic Research Foundation.

Supporting Information Available: Experimental details, a description of the FRAP analysis, and additional results. This material is available free of charge via the Internet at http://pubs.acs.org.

References

(1) Fang, Y.; Frutos, A. G.; Lahiri, J. *J. Am. Chem. Soc.* **2002**, *124*, 2394−2395.
(2) Simons, K.; Ikonen, E. *Nature* **1997**, *387*, 569−572.
(3) Salaun, C.; James, D. J.; Chamberlain, L. H. *Traffic* **2004**, *5*, 255−264.
(4) Campbell, S. M.; Crowe, S. M.; Mak, J. *J. Clin. Virol.* **2001**, *22*, 217−227.
(5) Fortin, D. L.; Troyer, M. D.; Nakamura, K.; Kubo, S.; Anthony, M. D.; Edwards, R. H. *J. Neurosci.* **2004**, *24*, 6715−6723.
(6) Mammen, M.; Choi, S.-K.; Whitesides, G. M. *Angew. Chem. Int. Ed.* **1998**, *37*, 2755−2794.
(7) Brian, A. A.; McConnell, H. M. *Proc. Natl. Acad. Sci. U.S.A.* **1984**, *81*, 6159−6163.
(8) Castellana, E. T.; Cremer, P. S. *Surf. Sci. Rep.* **2006**, *61*, 429−444.
(9) Richter, R. P.; Berat, R.; Brisson, A. R. *Langmuir* **2006**, *22*, 3497−3505.
(10) McConnell, H. M.; Watts, T. H.; Weis, R. M.; Brian, A. A. *Biochim. Biophys. Acta.* **1986**, *864*, 95−106.
(11) Salafsky, J.; Groves, J. T.; Boxer, S. G. *Biochemistry* **1996**, *35*, 14773−14781.
(12) Bockmann, R. A.; Hac, A.; Heimburg, T.; Grubmuller, H. *Biophys. J.* **2003**, *85*, 1647−1655.
(13) Seu, K. J.; Pandey, A. P.; Haque, F.; Proctor, E. A.; Ribbe, A. E.; Hovis, J. S. *Biophys. J.* **2007**, *92*, 2445−2450.
(14) Lahiri, J.; Kalal, P.; Frutos, A. G.; Jonas, S. T.; Schaeffler, R. *Langmuir* **2000**, *16*, 7805−7810.
(15) Atanasov, V.; Atanasova, P. P.; Vockenroth, I. K.; Knorr, N.; Koper, I. *Bioconjugate Chem.* **2006**, *17*, 631−637.
(16) Rossetti, F. F.; Bally, M.; Michel, R.; Textor, M.; Reviakine, I. *Langmuir* **2005**, *21*, 6443−6450.
(17) Keller, C. A.; Kasemo, B. *Biophys. J.* **1998**, *75*, 1397−1402.
(18) Nollert, P.; Kiefer, H.; Jahnig, F. *Biophys. J.* **1995**, *69*, 1447−1455.
(19) Horton, M. R.; Reich, C.; Gast, A. P.; Radler, J. O.; Nickel, B. *Langmuir* **2007**, *23*, 6263−6269.
(20) Reviakine, I.; Bergsma-Schutter, W.; Morozov, A. N.; Brisson, A. *Langmuir* **2001**, *17*, 1680−1686.
(21) Reviakine, I.; Brisson, A. *Langmuir* **2001**, *17*, 8293−8299.
(22) Larsson, C.; Rodahl, M.; Hook, F. *Anal. Chem.* **2003**, *75*, 5080−5087.
(23) Richter, R. P.; Him, J. L. K.; Tessier, B.; Tessier, C.; Brisson, A. R. *Biophys. J.* **2005**, *89*, 3372−3385.
(24) Vogel, J.; Bendas, G.; Bakowsky, U.; Hummel, G.; Schmidt, R. R.; Kettmann, U.; Rothe, U. *Biochim. Biophys. Acta−Biomembr.* **1998**, *1372*, 205−215.
(25) Shi, J.; Yang, T.; Kataoka, S.; Zhang, Y.; Diaz, A. J.; Cremer, P. S. *J. Am. Chem. Soc.* **2007**, *129*, 5954−5961.
(26) Johnson, J. M.; Ha, T.; Chu, S.; Boxer, S. G. *Biophys. J.* **2002**, *83*, 3371−3379.
(27) Morigaki, K.; Tawa, K. *Biophys. J.* **2006**, *91*, 1380−1387.
(28) Tawa, K.; Morigaki, K. *Biophys. J.* **2005**, *89*, 2750−2758.

(29) Leonenko, Z. V.; Carnini, A.; Cramb, D. T. *Biochim. Biophys. Acta—Biomembr.* **2000**, *1509*, 131−147.
(30) Schonherr, H.; Johnson, J. M.; Lenz, P.; Frank, C. W.; Boxer, S. G. *Langmuir* **2004**, *20*, 11600−11606.
(31) Keller, C. A.; Glasmastar, K.; Zhdanov, V. P.; Kasemo, B. *Phys. Rev. Lett.* **2000**, *84*, 5443−5446.
(32) Reimhult, E.; Larsson, C.; Kasemo, B.; Hook, F. *Anal. Chem.* **2004**, *76*, 7211−7220.
(33) Puu, G.; Gustafson, I. *Biochim. Biophys. Acta—Biomembr.* **1997**, *1327*, 149−161.
(34) Axelrod, D.; Koppel, D. E.; Schlessinger, J.; Elson, E.; Webb, W. W. *Biophys. J.* **1976**, *16*, 1055−1069.
(35) Patel, A. R.; Frank, C. W. *Langmuir* **2006**, *22*, 7587−7599.
(36) Magde, D.; Webb, W. W.; Elson, E. *Phys. Rev. Lett.* **1972**, *29*, 705.
(37) Cooper, M. A. *J. Mol. Recognit.* **2004**, *17*, 286−315.
(38) Dahlin, A.; Zach, M.; Rindzevicius, T.; Kall, M.; Sutherland, D. S.; Hook, F. *J. Am. Chem. Soc.* **2005**, *127*, 5043−5048.
(39) Haes, A. J.; Chang, L.; Klein, W. L.; Van Duyne, R. P. *J. Am. Chem. Soc.* **2005**, *127*, 2264−2271.
(40) Haes, A. J.; Van Duyne, R. P. *J. Am. Chem. Soc.* **2002**, *124*, 10596−10604.
(41) Haes, A. J.; Van Duyne, R. P. *Anal. Bioanal. Chem.* **2004**, *379*, 920−930.
(42) Larsson, E. M.; Alegret, J.; Kall, M.; Sutherland, D. S. *Nano Lett.* **2007**, *7*, 1256−1263.
(43) Riboh, J. C.; Haes, A. J.; McFarland, A. D.; Yonzon, C. R.; Van Duyne, R. P. *J. Phys. Chem. B* **2003**, *107*, 1772−1780.
(44) Sherry, L. J.; Jin, R. C.; Mirkin, C. A.; Schatz, G. C.; Van Duyne, R. P. *Nano Lett.* **2006**, *6*, 2060−2065.
(45) Stewart, M. E.; Mack, N. H.; Malyarchuk, V.; Soares, J.; Lee, T. W.; Gray, S. K.; Nuzzo, R. G.; Rogers, J. A. *Proc. Natl. Acad. Sci. U.S.A.* **2006**, *103*, 17143−17148.
(46) Yonzon, C. R.; Stuart, D. A.; Zhang, X. Y.; McFarland, A. D.; Haynes, C. L.; Van, Duyne, R. P. *Talanta* **2005**, *67*, 438−448.
(47) Englebienne, P. *Analyst* **1998**, *123*, 1599−1603.
(48) Nath, N.; Chilkoti, A. *Anal. Chem.* **2002**, *74*, 504−509.
(49) Jensen, T. R.; Malinsky, M. D.; Haynes, C. L.; Van Duyne, R. P. *J. Phys. Chem. B* **2000**, *104*, 10549−10556.
(50) Chumanov, G.; Sokolov, K.; Gregory, B. W.; Cotton, T. M. *J. Phys. Chem.* **1995**, *99*, 9466−9471.
(51) Curry, A.; Nusz, G.; Chilkoti, A.; Wax, A. *Opt. Express* **2005**, *13*, 2668−2677.
(52) Dahlin, A. B.; Tegenfeldt, J. O.; Hook, F. *Anal. Chem.* **2006**, *78*, 4416−4423.
(53) Duval, M. M.; Kelly, K. L.; Schatz, G. C.; Van Duyne, R. P. *J. Phys. Chem. B* **2001**, *105*, 2343−2350.
(54) Miller, M. M.; Lazarides, A. A. *J. Phys. Chem. B* **2005**, *109*, 21556−21565.
(55) Olofsson, L.; Rindzevicius, T.; Pfeiffer, I.; Kall, M.; Hook, F. *Langmuir* **2003**, *19*, 10414−10419.
(56) El-Sayed, I. H.; Huang, X.; El-Sayed, M. A. *Nano Lett.* **2005**, *5*, 829−834.
(57) El-Sayed, I. H.; Huang, X.; El-Sayed, M. A. *Cancer Lett.* **2006**, *239*, 129−135.
(58) Jain, P. K.; El-Sayed, I. H.; El-Sayed, M. A. *Nano Today* **2007**, *2*, 18−29.
(59) Kumar, S.; Harrison, N.; Richards-Kortum, R.; Sokolov, K. *Nano Lett.* **2007**, *7*, 1338−1343.
(60) Shin, Y.-B.; Lee, J.-M.; Park, M.-R.; Kim, M.-G.; Chung, B. H.; Pyo, H.-B.; Maeng, S. *Biosens. Bioelectron.* **2007**, *22*, 2301−2307.
(61) McFarland, A. D.; Van Duyne, R. P. *Nano Lett.* **2003**, *3*, 1057−1062.
(62) Rindzevicius, T.; Alaverdyan, Y.; Dahlin, A.; Hook, F.; Sutherland, D. S.; Kall, M. *Nano Lett.* **2005**, *5*, 2335−2339.
(63) Raschke, G.; Kowarik, S.; Franzl, T.; Sonnichsen, C.; Klar, T. A.; Feldmann, J.; Nichtl, A.; Kurzinger, K. *Nano Lett.* **2003**, *3*, 935−938.
(64) Haes, A. J.; Zou, S. L.; Schatz, G. C.; Van Duyne, R. P. *J. Phys. Chem. B* **2004**, *108*, 109−116.
(65) Dahlin, A. B.; Jonsson, M.; Höök, F. **2007**, submitted for publication.
(66) Rodolphe, M.; Andreas, B. D.; Jonas, O. T.; Fredrik, H. *Biointerphases* **2007**, *2*, 49−55.
(67) Hanarp, P.; Sutherland, D. S.; Gold, J.; Kasemo, B. *Colloids Surf. A* **2003**, *214*, 23−36.
(68) Haes, A. J.; Zou, S. L.; Schatz, G. C.; Van Duyne, R. P. *J. Phys. Chem. B* **2004**, *108*, 6961−6968.
(69) Prikulis, J.; Hanarp, P.; Olofsson, L.; Sutherland, D.; Kall, M. *Nano Lett.* **2004**, *4*, 1003−1007.
(70) Johnson, P. B.; Christy, R. W. *Phys. Rev. B* **1972**, *6*, 4370−4379.
(71) Weng, K. C.; Stalgren, J. J. R.; Duval, D. J.; Risbud, S. H.; Frank, C. W. *Langmuir* **2004**, *20*, 7232−7239.
(72) Reviakine, I.; Brisson, A. *Langmuir* **2000**, *16*, 1806−1815.
(73) Reimhult, E.; Hook, F.; Kasemo, B. *Langmuir* **2003**, *19*, 1681−1691.
(74) Reimhult, E.; Zach, M.; Hook, F.; Kasemo, B. *Langmuir* **2006**, *22*, 3313−3319.
(75) Barnes, W. L.; Dereux, A.; Ebbesen, T. W. *Nature* **2003**, *424*, 824−830.
(76) Reinhard, B. M.; Sheikholeslami, S.; Mastroianni, A.; Alivisatos, A. P.; Liphardt, J. *Proc. Natl. Acad. Sci. U.S.A.* **2007**, *104*, 2667−2672.
(77) Kunneke, S.; Janshoff, A. *Angew. Chem., Int. Ed.* **2001**, *41*, 314−316.

NL072006T